13th International Symposium on Particle Image Velocimetry – ISPIV 2019
Munich, Germany, July 22-24, 2019

Soap bubbles for volumetric velocity measurements in air flows

Diogo Barros[1,2*], Yanchong Duan[4], Daniel Troolin[3]
Ellen K. Longmire[1], Wing Lai[3]

[1] University of Minnesota, Aerospace Engineering and Mechanics, Minneapolis, MN 55455, USA

[2] Aix-Marseille Université, CNRS, IUSTI, Marseille, France

[3] TSI, Incorporated, 500 Cardigan Rd., Shoreview, MN, USA

[4] State Key Laboratory of Hydroscience and Engineering, Tsinghua University, Beijing 100084, China

[*] diogo.camello-barros@univ-amu.fr

Abstract

The use of air-filled soap bubbles with diameter 10-30μm is demonstrated for volumetric velocimetry in air flows covering domains of 75-490 cm^3. The tracers are produced by a novel system that seeds high-density soap bubble streams for particle image velocimetry applications. Particle number density considerations, spatial resolution and response time scales are discussed in light of current seeding techniques for volumetric measurements. Finally, the micro soap bubbles are employed to measure the 3D velocity field in the wake of a sphere immersed in a turbulent boundary layer.

1 Introduction

Volumetric velocimetry is a key enabler for understanding turbulent flows, which are inherently unsteady and three-dimensional. Multiple methods have been designed to measure 3D velocity fields accurately. In particular, particle image velocimetry (PIV) and particle tracking velocimetry (PTV) are now widely employed in various flow configurations (Discetti and Coletti, 2018). All of these techniques rely on imaging of discrete seeding tracers suspended in the flow. While larger seeding particles scatter more light from the illuminating source, smaller ones follow the flow more accurately and can resolve smaller scale variations. This trade off is inherent to particle-based velocimetry (Melling, 1997).

Current seeding tracers for air flows include oil and di-ethyl-hexyl-sebacic acid-ester (DEHS) droplets as well as soap bubbles filled with a low-density gas such as helium. While droplets of size 1μm typically can follow fluid elements faithfully and remain suspended in the flow, the maximum size of the volumetric domain considered is usually limited to smaller than 50 cm^3 (Scarano, 2012). On the other hand, large helium-filled soap bubbles (HFSB) ranging from 1 mm to 5 mm allow only qualitative investigation of larger domains, as they do not faithfully follow the flow like neutrally buoyant bubbles (Kerho and Bragg, 1994). Sub millimeter (300μm) helium-filled soap bubbles have also been utilized for large-scale aerodynamic applications (Scarano et al., 2015) in domains larger than 4500 cm^3, in both low and high-speed tomo-PIV configurations.

A compilation of volumetric measurements in air flows using these seeding strategies is shown in figure 1. There is a noticeable gap between volumetric domains in the range between nearly 50 cm^3 and 5000 cm^3. This is an effect of the large difference between the mean seeding diameters of DEHS droplets and HFSB bubbles. The purpose of the current work is to demonstrate the viability of smaller size air-filled soap bubbles as seeding tracers in gas volumes of intermediate size. The bubbles are generated by the rapid depressurization of a pressurized mixture of liquid and surfactant. The depressurization causes the gas to leave the liquid media. This controlled degasification inside a reservoir produces a large number of soap bubbles with mean diameter of 15μm. The bubbles can be imaged easily either by low or high-speed light sources, yet they are small enough to resolve turbulent flow structures in intermediate-size domains.

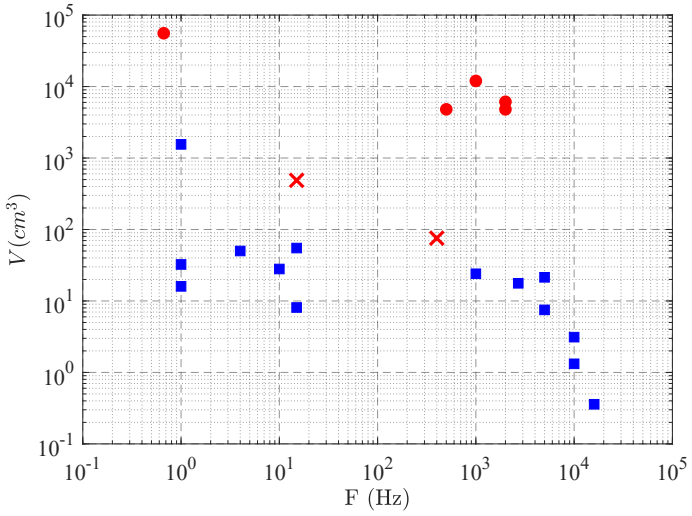

Figure 1: Compilation of volumetric velocimetry investigations in air flows: acquisition frequency of the PIV set-up and the imaged volume. References: (Atkinson et al., 2011), (Kühn et al., 2011), (Cafiero et al., 2015),(Caridi et al., 2016), (Boushaki et al., 2017), (Pröbsting et al., 2013), (Ghaemi and Scarano, 2011), (Schneiders et al., 2016; Schneiders and Scarano, 2016), (Elsinga et al., 2006), (Schröder et al., 2008), (Humble et al., 2009), (Terra et al., 2017, 2018), (Scarano et al., 2015), (Violato et al., 2011), (Michaelis et al., 2012), (Fukuchi, 2012) and (Staack et al., 2010). The squares represent volumetric measurements using seeding particles with diameter of about $1\mu m$, while the circles indicate investigations where HFSB were used. The crosses represent the two volumetric domains considered in the present work.

The paper is organized as follows. In section §2, we discuss spatial and time scale considerations for volumetric velocimetry in air flows, focusing on the seeding size and properties. The methodology to generate the soap bubbles and their characteristics are outlined in §3. A demonstration of the use of micro soap bubbles in a wind-tunnel is provided in section §4. Finally, our concluding remarks and perspectives on these new seeding tracers are discussed.

2 Considerations of seeding size and 3D velocimetry

Two seeding limits must be considered to obtain 3D velocity fields. First, for a given volume and optical system, the particles should be large enough to be imaged by the camera sensors. Second, to increase the spatial resolution of the resulting volumetric field, one should maximize the number of identifiable particles in 3D sub-domains (voxels, for 3D-PIV or particle separation, for PTV based methods) by decreasing the diameter of the seeding tracers and the number of pixels they occupy in the camera images. For a given imaging system, we address the following questions: in a volumetric domain, what is the minimum seeding tracer diameter necessary to obtain a sufficient number of image pixels in the camera sensor? Then, how to relate the spatial resolution of the velocity measurements with the seeding size?

Let us consider a camera with a pixel resolution l^*, pixel pitch Δ_{pix} equipped with an optical system with numerical aperture $f_\#$ imaging a volume $V = L \times H \times W$ by the use of an illuminating source with wavelength λ.

The optical magnification is given by

$$M = \frac{l^* \Delta_{\text{pix}}}{L} \tag{1}$$

and the depth of focus reads

$$\Delta Z = 4.88 {f_\#}^2 \lambda \left(1 + \frac{1}{M}\right)^2. \tag{2}$$

Let d_p be the diameter of the seeding particle. The pixel normalized image diameter in the camera sensor can be calculated from

$$d_\tau{}^* = \frac{\sqrt{(Md_p)^2 + d_{\text{diff.}}{}^2 + d_B{}^2}}{\Delta_{\text{pix}}}, \tag{3}$$

where $d_{\text{diff.}} = 2.44\lambda f_\#(1+M)$ is the diffraction limited minimum image diameter and d_B is the blur circle diameter (Raffel et al., 2018; Scarano, 2012).

By imposing a minimum image diameter $d_\tau{}^*$ required to identify and to track the tracer, we obtain the minimum physical tracer diameter

$$d_{p_{\min}} = \sqrt{\frac{(d_\tau{}^*\Delta_{\text{pix}})^2 - d_{\text{diff.}}{}^2 - (d_B{}^*\Delta_{\text{pix}})^2}{M}}. \tag{4}$$

Let us take the example of the experiments performed in Scarano et al. (2015) with HFSB bubbles. The illuminated volume was such that $L = H = 200\,\text{mm}$, $W = 120\,\text{mm}$, $l^* = 1024\,\text{px}$, $\Delta_{\text{pix}} = 20\,\mu\text{m}$ and $f_\# = 32$ to ensure focus along all the depth W ($\Delta Z \sim 300\,\text{mm}$). Assuming $d_\tau{}^* = 3\,\text{px}$ and the blur circle of $d_B{}^* = 1\,\text{px}$, we obtain $d_p \sim 320\,\mu\text{m}$, a consistent value when compared to the actual size of the helium bubbles. Now, decreasing the domain size to $L = H = 60\,\text{mm}$ while keeping all other parameters the same requires a minimum particle diameter of about $d_p \sim 30\,\mu\text{m}$ with $\Delta Z \sim 40\,\text{mm}$, i.e. an equivalent volume of approximately $V \sim 140\,\text{cm}^3$ when compared to $V \sim 4800\,\text{cm}^3$ from Scarano et al. (2015). These examples clearly show that, to achieve intermediate volumetric domains, seeding tracers with diameter an order of magnitude smaller than HFSB are preferable, but still much larger than DEHS droplets used for smaller domains.

We consider now the same domain $V = L \times H \times W$ divided in voxels. We define l_{IB} as the length of the interrogation box (IB), i.e. the spatial resolution of the particle-based velocimetry. The number of seeding particles within the interrogation box is given by:

$$N_{p_{\text{IB}}} = n_{v_{\text{IB}}} \times PPV. \tag{5}$$

Here, $n_{v_{\text{IB}}}$ is the number of voxels per interrogation box, while PPV is the number of particles per voxel. Considering the volumetric particle concentration $C = N_p/V$, PPV reads

$$PPV = C\left(\frac{\Delta_{\text{pix}}}{M}\right)^3. \tag{6}$$

By writing the particle concentration C as a function of the source density N_s (Scarano, 2012) and particle diameter $d_\tau^\star$, we obtain:

$$C = \frac{N_s}{W}\left(\frac{M}{\Delta_{\text{pix}}}\right)^2 \frac{4}{\pi {d_\tau{}^*}^2}. \tag{7}$$

Then, the number of particles per interrogation box reads

$$N_{p_{\text{IB}}} = n_{v_{\text{IB}}} \frac{N_s}{W}\left(\frac{\Delta_{\text{pix}}}{M}\right) \frac{4}{\pi {d_\tau{}^*}^2}. \tag{8}$$

Assuming $n_{v_{\text{IB}}} = (l_{\text{IB}}/l_v)^3$, where l_v is the voxel length, and noting that $\frac{l_v M}{\Delta_{\text{pix}}} = 1$, we write

$$l_{\text{IB}} = \left(\frac{\pi}{4}\frac{N_{p_{\text{IB}}}}{N_s} d_\tau{}^2 W\right)^{1/3}. \tag{9}$$

Finally, for a desired number of particles per IB, usually between 5 and 10 particles (Scarano, 2012) we note that

$$l_{\text{IB}} \propto d_\tau{}^{\frac{2}{3}} N_s{}^{-\frac{1}{3}}. \tag{10}$$

While the source density will be set to a limit to increase the accuracy of the tomographic reconstruction, decreasing the particle size may reduce the IB length scale or increase the PIV spatial resolution. Thus, for intermediate sized volumes, there will be a substantial gain in the number of velocity vectors by decreasing d_p from 300μm to 30μm, for example.

3 Description of the current seeding methodology

3.1 Hardware description

In conventional methods of generating bubbles, an air stream is pushed (or blown) through a liquid film. An illustrative example of this process is making soap bubbles by blowing air through a film of soap that is formed on a wire frame. The size of the wire frame (or orifice diameter in cases that a nozzle is used) determines the limiting dimension of the bubbles produced. The method described here overcomes this limitation by using the process of cavitation in liquid media. The basic concept relies on the rapid depressurization of an already pressurized mixture of liquid containing a desired amount of surfactants (or any liquid with surface tension less than that of pure water). The current device consists of a 15 gallon (57 liters) reservoir filled approximately one-third full with a 5% water-surfactant solution. A drain at the bottom of the reservoir feeds the solution through a set of particulate filters and then to a reciprocating piston pump that pressurizes the fluid to about 70 bars (or 1000 psi).

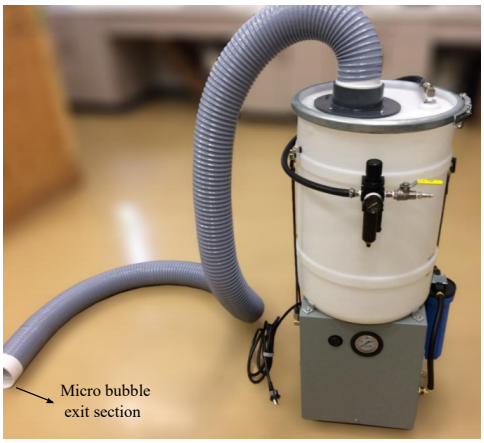

Figure 2: Micro bubble generator.

The pressurized liquid then travels through high-pressure tubing to a set of 10 nozzles with orifice diameter of less than 1 mm. The water-surfactant solution and dissolved air rapidly expand at the nozzle exit and then collapse due to the cavitation process. The implosion process of the bubbles further fragments the initial bubble into many smaller micron-sized bubbles. The bubble plume is exhausted from the nozzles into the reservoir which contains an opening at the top. Pressurized air is introduced into the reservoir in order to force the bubbles out, while simultaneously creating a mild cyclonic flow within the chamber that causes larger bubbles and droplets to impact the sidewalls and become reintroduced into the solution. The bubbles that escape are primarily neutrally buoyant and most of the bubbles created in this way remain suspended for long periods of time.

3.2 Bubble characterization

Figure 3(left) shows bubbles imaged using a high magnification lens. In order to characterize the bubble size, a phase Doppler particle analysis (PDPA) system was used (Bachalo, 1980). PDPA uses a set of crossed laser beams to create an interference fringe pattern at the point where the beams cross. Spherical particles passing through the beam crossing scatter light collected by a receiver with an array of three detectors. The phase lag of the scattered light between detectors is proportional to the particle diameter.

A flexible tube 10 cm in diameter and 3 meters long was attached to the exit on top of the bubble generator. The PDPA system was positioned to measure the bubbles as they exited the tube. The generator

Table 1: Stokes number and relaxation times for several tracers including the micro-bubbles of the current study.

Seeding tracer	Density (kg.m^{-3})	Diameter (μm)	St_K (1 kHz)	Response time τ_p (μs)
DEHS	912	1	0.01	3
Olive oil	917	1	0.01	3
Current study	40	15	0.12	28
HFSB	1.1	500	4.14	844
Air bubbles	4.4	400	3.31	2161

produced a concentration of bubbles on the order of 10^7 bubbles per second at the measurement volume. Figure 3(right) shows the measured diameter distribution of the bubbles generated by the device. The mean diameter was $14.7\,\mu m$ with a standard deviation of $7.3\,\mu m$.

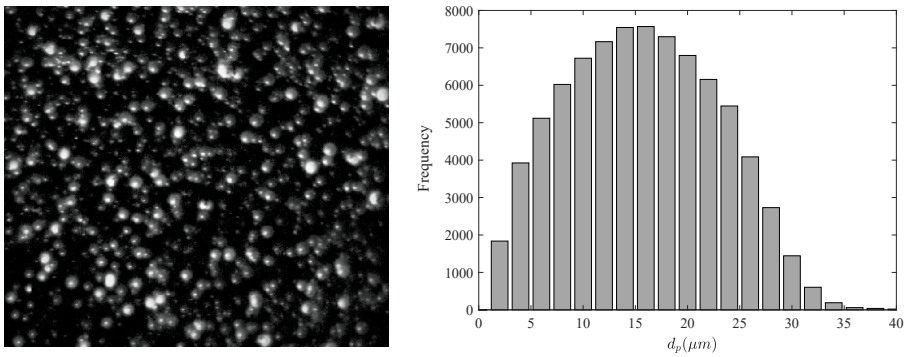

Figure 3: High-resolution image of micro soap bubbles (left) and their size distribution (right).

3.3 Bubble response time

A primary factor that affects the ability of the particle to follow the flow in a faithful manner is the drag force acting on the particle. Relaxation time (or, response time) and Stokes number are related to the fidelity of tracer particles accurately following the flow. Relaxation time (τ_p) represents the characteristic time required for a tracer particle to reach an equilibrium condition after a flow disturbance. The relaxation time is commonly calculated using the following form

$$\tau_p = {d_p}^2 \frac{\rho_p}{18\mu}, \tag{11}$$

where d_p is the particle diameter, ρ_p the particle density and μ the dynamic viscosity of the ambient fluid.

The Stokes number (St_K) is defined as the ratio of the characteristic time of a particle to a characteristic time of the flow. The commonly used definitions for these quantities are listed according to those given in Melling (1997); Raffel et al. (2018). The values for relaxation time and Stokes number for various particles are given in table 1. Here, the value of St_K is obtained based on the flow time scale associated to motions of 1 kHz frequency.

The Stokes number of the micro-bubbles was found to be $St_K \sim 0.12$. In general, a Stokes number of 0.1 or less is desired for particles to faithfully follow the flow (Tropea and Yarin, 2007).

4 Results and conclusions

Experiments were conducted in two wind-tunnels of the Department of Aerospace Engineering and Mechanics of the University of Minnesota. Preliminary tests demonstrated the capability of performing large-scale

volumetric measurements within a domain of 490 cm^3 in a closed-circuit wind-tunnel. This volume lies between the traditional volumetric domains investigated using either DEHS droplets or HSFB bubbles. After filling the tunnel with bubbles, the bubble generator was turned off for the bubbles to recirculate for 5 minutes. Then a timer was started and bubble concentration measurements were performed. After an additional 5, 10, and 20 minutes, 64%, 47%, and 33% of the bubbles remained, respectively.

Another set of experiments was performed in an open-circuit wind-tunnel as shown in figure 4(a). A trip wire was placed at the entrance of the wind tunnel to generate a turbulent boundary layer. The wind tunnel has a cross section of 600×600 mm and a maximum flow speed of 40 ms^{-1}. The wind tunnel was driven by a frequency controlled variable speed motor and operated here with a fixed free-stream velocity U_o of 3 ms^{-1}. The estimated friction Reynolds number of the developing turbulent boundary layer is $Re_\tau = 500$.

For volumetric velocity measurements, a V3V-Flex system from TSI Incorporated was employed and displaced according to the sketch of figures 4(a,b). Four 4MP cameras (Cam1 to Cam4, 2560×1600 pixels) equipped with Scheimpflug adapters were aligned in a planar configuration to image the illuminated volume. Each camera was equipped with a 135 mm lens and the f-number was set individually to consider the forward/backward scattering effects (forward scattering: Cam1 and Cam4; backward scattering: Cam2 and Cam4). The measuring volume was illuminated by a 30mJ/pulse dual-head Nd:YLF laser positioned at the open outlet of the wind tunnel. The volume of interest (VOI, dimensions $90 \times 56 \times 15$ mm^3) was located 1650 mm downstream of the trip wire with its side plane lies in the center line of the wind tunnel. A timing box was used to synchronize the laser pulses and the cameras. Throughout this section, the streamwise, wall-normal, and spanwise directions are denoted by x, y, and z, respectively. The instantaneous velocity fluctuations in the corresponding directions are denoted by u, v and w, while the associated mean velocities are defined by U, V and W, respectively. All quantities normalized by the boundary layer friction velocity u_τ and the kinematic viscosity ν are denoted with a superscript $+$. The root mean square value of a quantity is denoted by a prime ($'$) and its ensemble average is represented by an angle bracket $(<>)$.

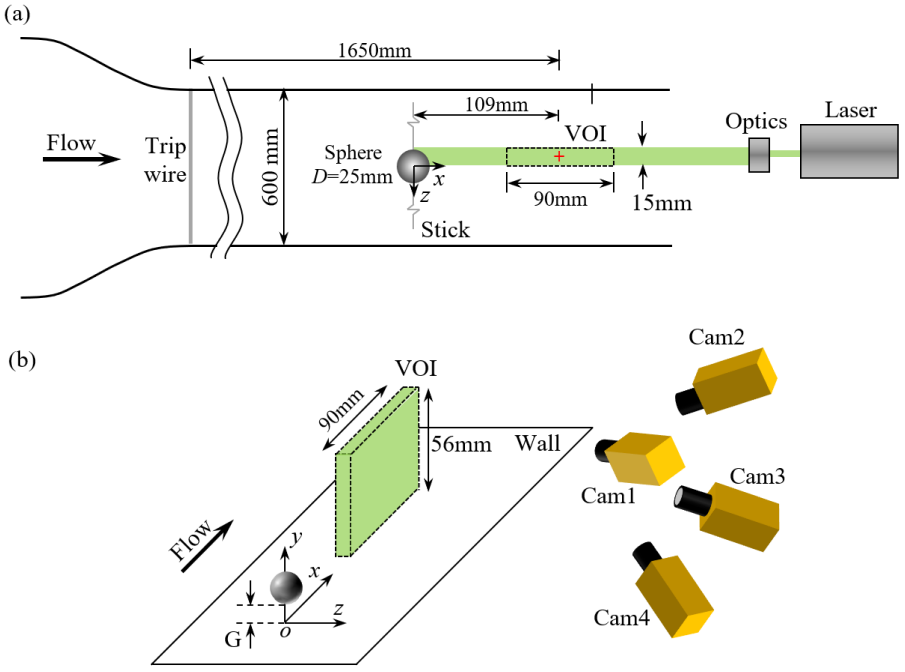

Figure 4: Sketch of the experimental setup. (a) Top view of the wind tunnel; (b) 3D view of the coordinate system and arrangement of cameras, sphere, and VOI.

Measurements were conducted at two flow configurations: free-stream (FS) and sphere-perturbed (SP) turbulent boundary layer. For the SP case, a sphere (diameter $D = 25$ mm, $D^+ = 240$) fixed by a spanwise stick was placed inside the test section 109 mm upstream of the VOI center location (see red cross in figure 4(a)). Two SP cases were considered by changing the gap distance G between the bottom of the sphere and the wall, G =0 and R, where R is the sphere radius. These two configurations are denoted as SP-G0 and SP-GR, respectively. In all cases, the time interval between successive frames was 150 μs and two sampling

frequencies 60 Hz and 400 Hz were selected.

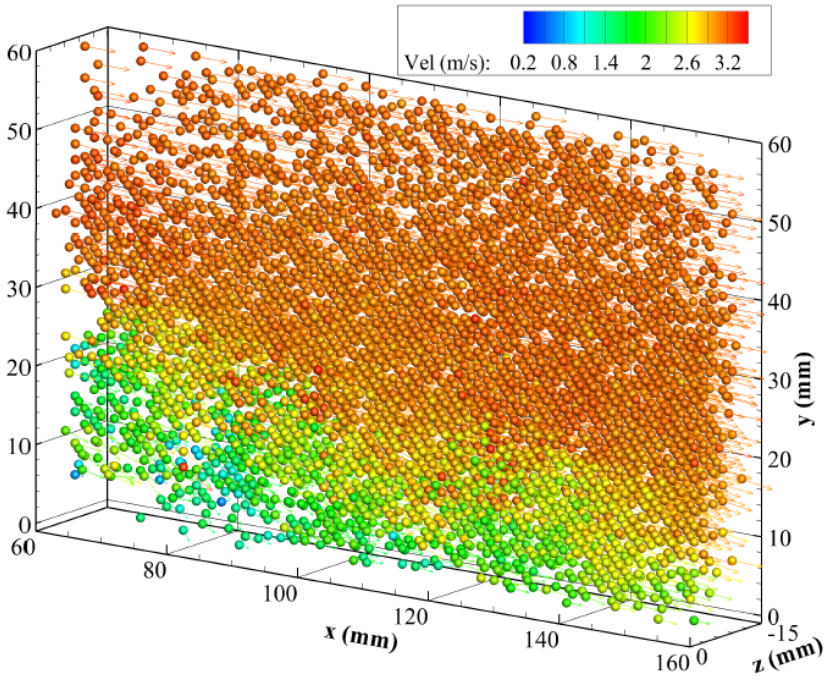

Figure 5: Binned vectors in a uniform grid.

Both the calibration and image processing steps prior to volumetric velocity computation were performed in Insight V3V 4G. For image processing, the raw images were pre-processed using the following steps to reduce background and noise effects: 1) apply a 3×3 pixels Gaussian filter to remove the noise; 2) subtract a local median (9×9 pixels) to remove the background; 3) subtract a constant intensity of 10 and multiply by a constant value of 5 to increase the contrast; 4) apply a 7×7 pixels Gaussian filter to facilitate the particle identification process. For each snapshot, the number of identified bubbles within the VOI was in the range 5000-8000. The 3D velocity vectors associated to these bubbles were binned into a uniform grid with removed bad vectors (exceeding the mean value $\pm$ three times the standard deviation in each bin) to obtain the flow fields with a uniform vector spacing of $2 \times 2 \times 2\,\mathrm{mm}^3$. The outliers of these flow fields at each grid point were further removed (exceeding the mean value $\pm\ \beta$ times the standard deviation, where $\beta = 3$ for u and v components, $\beta = 2$ for w given the higher uncertainty for the w component). Figure 5 shows an instantaneous snapshot of the binned velocity vector field.

The capability of the micro soap bubbles was first investigated under the free-stream condition by comparing the statistical velocity profiles with results from direct numerical simulations (DNS) of a turbulent boundary layer at similar Reynolds numbers ($Re_\tau = 580$). The numerical data set is extracted from Jiménez et al. (2010). As presented in figure 6, the profiles of the mean streamwise velocity U, the velocity fluctuations (u', v' and w') and the Reynolds shear stress $< uv >$ agree quite well with those from the DNS, thus validating the turbulent boundary layer condition.

Figure 7 depicts two flow snapshots each of the sphere-perturbed configurations (SP-G0 and SP-GR). In the case where the sphere is close to the wall (SP-G0), the majority of vortical structures induced by the sphere are located within $0 < y < D$. Also, these shed structures present mainly a negative vorticity sign (clockwise rotation), while alternating vortices are shed from the sphere for the SP-GR configuration shown in figures 7(b,d). In this case, the vortical activity is spread across the region within $0.5D < y < 2D$. The complexity of the vorticity field can be explained by the combination of vortices convected within the turbulent boundary layer, the ejected fluid below the sphere and the vortex shedding downstream of the sphere.

The current experiments demonstrate the feasibility of volumetric velocity measurements in air flows within intermediate-sized volumes using micro soap bubbles. The mean diameter of these bubbles being approximately $15\,\mu m$ allows one to resolve smaller scales of the flow field, as demonstrated here for the case of a sphere wake immersed in a turbulent boundary layer. Both the wake structures and the boundary

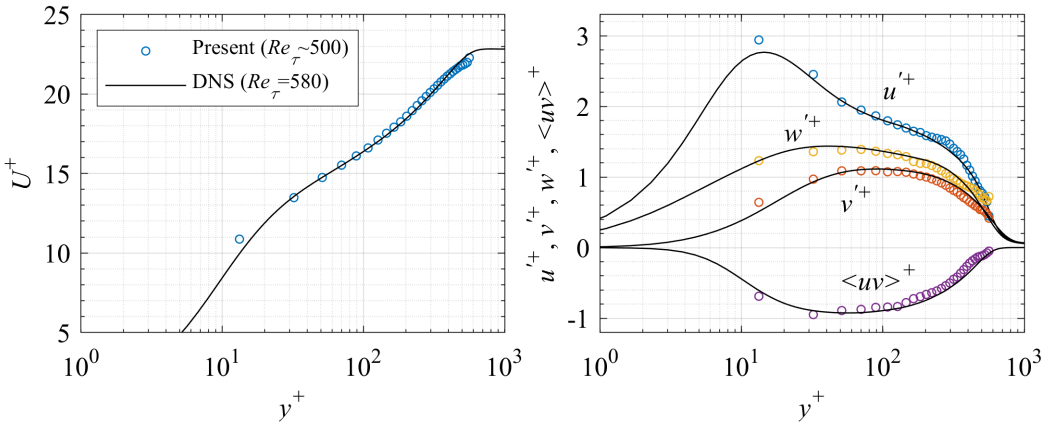

Figure 6: Wall-normal velocity profiles of the inner scaled (a) streamwise velocity, (b) turbulent intensities and Reynolds shear stress for the free-stream condition.

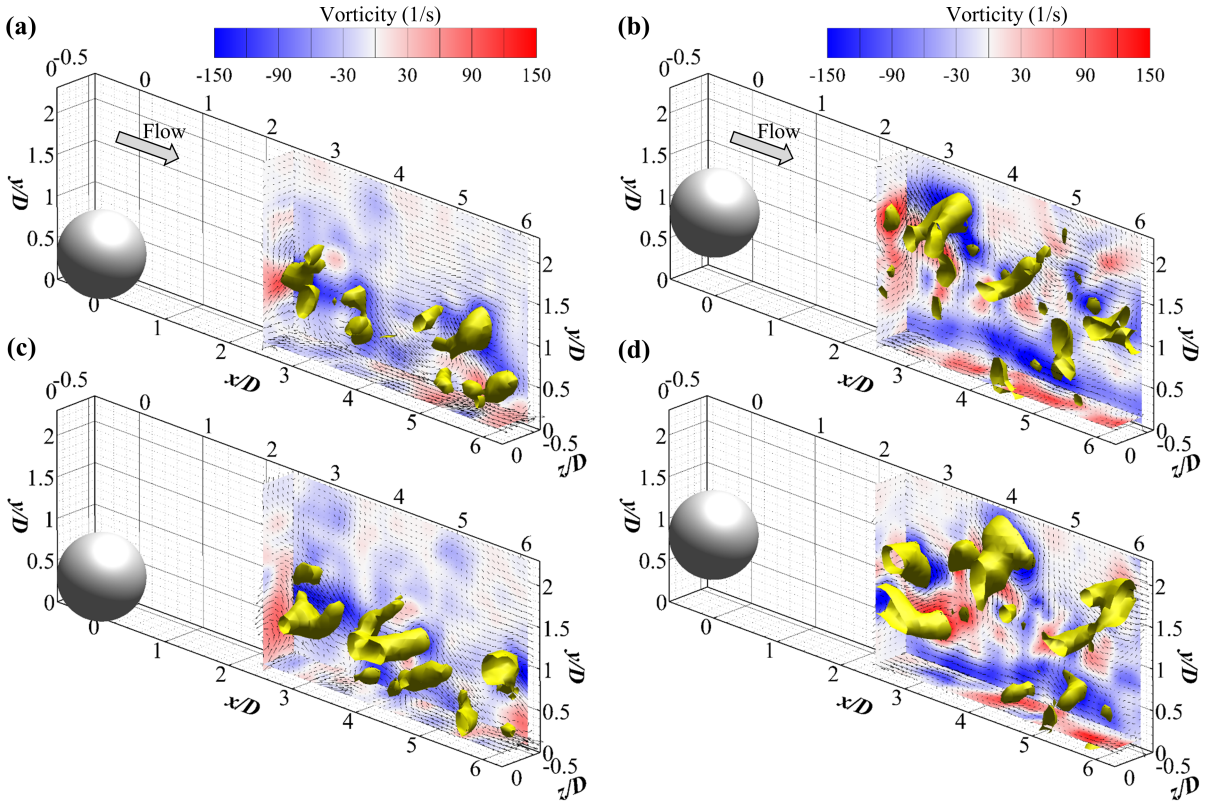

Figure 7: Instantaneous flow fields for sphere-perturbed configurations. (a,c): SP-G0; (b,d): SP-GR. The top and bottom rows are two instants with time separation $\Delta t^+ = 13$. The vectors on each plane are the in-plane fluctuating velocities while the color denotes the out of plane component of vorticity. The yellow iso-surface depicts flow structures identified with the Q-criterion where $Q = 2000\,\mathrm{s}^{-2}$.

layer statistics were successfully measured with a reasonably good spatial resolution. This seeding methodology thus complements the current methods for volumetric measurements in air flows for the range of intermediate-size volumes. In addition, it provides high-density seeding for further particle tracking and time-resolved velocimetry techniques (Schanz et al., 2016).

Acknowledgements

This work was supported by TSI Incorporated. This work was partially supported by the U.S. National Science Foundation (NSF CBET-1510154).

References

Atkinson C, Coudert S, Foucaut JM, Stanislas M, and Soria J (2011) The accuracy of tomographic particle image velocimetry for measurements of a turbulent boundary layer. *Experiments in Fluids* 50:1031–1056

Bachalo WD (1980) Method for measuring the size and velocity of spheres by dual-beam light-scatter interferometry. *Applied Optics* 19:363–370

Boushaki T, Koched A, Mansouri Z, and Lespinasse F (2017) Volumetric velocity measurements (V3V) on turbulent swirling flows. *Flow Measurement and Instrumentation* 54:46–55

Cafiero G, Discetti S, and Astarita T (2015) Flow field topology of submerged jets with fractal generated turbulence. *Physics of Fluids* 27:115103

Caridi GCA, Ragni D, Sciacchitano A, and Scarano F (2016) Hfsb-seeding for large-scale tomographic PIV in wind tunnels. *Experiments in Fluids* 57:190

Discetti S and Coletti F (2018) Volumetric velocimetry for fluid flows. *Measurement Science and Technology* 29:042001

Elsinga GE, Scarano F, Wieneke B, and van Oudheusden BW (2006) Tomographic particle image velocimetry. *Experiments in Fluids* 41:933–947

Fukuchi Y (2012) Influence of number of cameras and preprocessing for thick volume tomographic PIV. in *16th International Symposium on Applications of Laser Techniques to Fluid Mechanics, Lisbon, Portugal*

Ghaemi S and Scarano F (2011) Counter-hairpin vortices in the turbulent wake of a sharp trailing edge. *Journal of Fluid Mechanics* 689:317–356

Humble R, Elsinga G, Scarano F, and Van Oudheusden B (2009) Three-dimensional instantaneous structure of a shock wave/turbulent boundary layer interaction. *Journal of Fluid Mechanics* 622:33–62

Jiménez J, Hoyas S, Simens MP, and Mizuno Y (2010) Turbulent boundary layers and channels at moderate reynolds numbers. *Journal of Fluid Mechanics* 657:335–360

Kerho MF and Bragg MB (1994) Neutrally buoyant bubbles used as flow tracers in air. *Experiments in Fluids* 16:393–400

Kühn M, Ehrenfried K, Bosbach J, and Wagner C (2011) Large-scale tomographic particle image velocimetry using helium-filled soap bubbles. *Experiments in Fluids* 50:929–948

Melling A (1997) Tracer particles and seeding for particle image velocimetry. *Measurement Science and Technology* 8:1406

Michaelis D, Bomphrey R, Henningsson P, and Hollis D (2012) Reconstructing the vortex skeleton of the desert locust using phase averaged POD approximations from time resolved thin volume tomographic PIV. in *16th International Symposium on Applications of Laser Techniques to Fluid Mechanics, Lisbon, Portugal*

Pröbsting S, Scarano F, Bernardini M, and Pirozzoli S (2013) On the estimation of wall pressure coherence using time-resolved tomographic PIV. *Experiments in Fluids* 54:1567

Raffel M, Willert CE, Scarano F, Kähler CJ, Wereley ST, and Kompenhans J (2018) *Particle image velocimetry: a practical guide*. Springer

Scarano F (2012) Tomographic PIV: principles and practice. *Measurement Science and Technology* 24:012001

Scarano F, Ghaemi S, Caridi CG, Bosbach J, Dierksheide U, and Sciacchitano A (2015) On the use of helium-filled soap bubbles for large-scale tomographic PIV in wind tunnel experiments. *Experiments in Fluids* 56:42

Schanz D, Gesemann S, and Schröder A (2016) Shake-the-box: Lagrangian particle tracking at high particle image densities. *Experiments in Fluids* 57:70

Schneiders JF, Caridi GC, Sciacchitano A, and Scarano F (2016) Large-scale volumetric pressure from tomographic PTV with HFSB tracers. *Experiments in Fluids* 57:164

Schneiders JF and Scarano F (2016) Dense velocity reconstruction from tomographic PTV with material derivatives. *Experiments in Fluids* 57:139

Schröder A, Geisler R, Elsinga GE, Scarano F, and Dierksheide U (2008) Investigation of a turbulent spot and a tripped turbulent boundary layer flow using time-resolved tomographic PIV. *Experiments in Fluids* 44:305–316

Staack K, Geisler R, Schröder A, and Michaelis D (2010) 3D-3C-coherent structure measurements in a free turbulent jet. in *15th International Symposium on Applications of Laser Techniques to Fluid Mechanics, Lisbon, Portugal*

Terra W, Sciacchitano A, and Scarano F (2017) Aerodynamic drag of a transiting sphere by large-scale tomographic-PIV. *Experiments in Fluids* 58:83

Terra W, Sciacchitano A, Scarano F, and van Oudheusden B (2018) Drag resolution of a PIV wake rake for transiting models. *Experiments in Fluids* 59:120

Tropea C and Yarin AL (2007) *Springer handbook of experimental fluid mechanics*. volume 1. Springer Science & Business Media

Violato D, Moore P, and Scarano F (2011) Lagrangian and eulerian pressure field evaluation of rod-airfoil flow from time-resolved tomographic PIV. *Experiments in Fluids* 50:1057–1070